Final Report

on the work performed at the University of Alabama in Huntsville

under NASA Grant **NAG8-1790**

Effects of convective transport of solute and impurities on defect-causing kinetics instabilities

Principal Investigator: Dr. Peter G. Vekilov

Assistant Professor of Chemistry

Period of Performance: **April 1, 1999 – August 31, 2001**

Huntsville, Alabama

August 31, 2001

Table of Contents

1. Development of Prototype Flight Hardware—Differential Phase Shifting Interferometer

For *in-situ* studies of the formation and evolution of step patterns during the growth of protein crystals, we have designed and assembled an experimental setup based on Michelson interferometry with the surface of the growing protein crystal as one of the reflective surfaces. The crystallization part of the device allows optical monitoring of a face of a crystal growing at temperature stable within 0.05 degrees Celsius in a developed solution flow of controlled direction and speed. The reference arm of the interferometer contains a liquid-crystal element that allows controlled shifts of the phase of the interferograms. We employ an image processing algorithm which combines five images with a $\pi/2$ phase difference between each pair of images. The images are transferred to a computer by a camera capable of capturing 6-8 frames per second. The device allows data collection data regarding growth over a relatively large area (approximately .3 sq. mm) *in-situ* and in real time during growth. The estimated dept resolution of the phase shifting interferometry is about 100 Å. The lateral resolution, depending on the zoom ratio, varies between 0.3 and 0.6 micrometers. We have now collected quantitative results on the onset, initial stages and development of instabilities in moving step trains on vicinal crystal surfaces at varying supersaturation, position on the facet, crystal size and temperature with the proteins ferritin, apoferritin and thaumatin. Comparisons with theory, especially with the AFM results on the molecular level processes, see below, allow tests of the rational for the effects of convective flows and, as a particular case, the lack thereof, on step bunching.

2. Other Experimental techniques developed and used in PI's Laboratory

Novel AFM imaging techniques

- *Molecular resolution imaging during growth.* Molecular resolution (1) images of proteins have been obtained before for two cases: (i) on flat crystal surfaces (2-6); or (ii) individual molecules strongly attached to a substrate (7, 8). We obtained molecular resolution images of *growing crystals* and visualized the edges of the unfinished crystal layers, a.k.a. growth step; incorporation of molecules into the steps constitutes the growth process. The *sites for incorporation* of the molecules, kinks, are located along the steps. Observations of the steps at molecular resolution allowed characterization of the growth processes *at a molecular, discrete level*, see Section5 below.
- *AFM movies with molecular resolution*: The time between AFM frames is ~ 20 s, comparable to average times for molecular incorporation. This method is similar to previous movies of equilibrium phenomena in ultrahigh vacuum (9-12). Using this method, we have seen attachment, detachment and reversible processes for single molecules, Section A.5 below and AFM movie at **http://www.cmmr.uah.edu/protein/movies.html**
- *Single-molecule manipulation* by applying a specified force on a select molecule on the surface with the AFM tip. A series of hits over a certain area on the crystal surface results in *etching* of a predefined number of molecules.
- We gained significant additional insight by extensively using two standard techniques of AFM data collection:

Tapping Mode imaging in solution (13-15) allows visualization of adsorbed protein and impurity species (tip impact in contact imaging mode often prevents such imaging). The tapping mode has also allowed us to see non-crystalline, glassy phases of proteins adsorbed on the substrate or on a crystal face, see Section A.6 below. In particular, this imaging mode helped us to visualize pre-nucleation and near-nucleation aggregates and in this way to monitor the nucleation pathways (16).
Scans with disabled y-axis, similar to observations in ultra-high vacuum by (9, 10, 12, 17-20). The technique allows monitoring of processes occurring in the millisecond range (21).

Publications:

Yau, S.-T., Thomas, B. R. & Vekilov, P. G. (2000). Molecular mechanisms of crystallization and defect formation. *Phys. Rev. Lett* **85**, 353-356.

Yau, S.-T., Petsev, D. N., Thomas, B. R. & Vekilov, P. G. (2000). Molecular-level thermodynamic and kinetic parameters for the self-assembly of apoferritin molecules into crystals. *J. Mol. Biol* **303** (5), 667-678 (2000).

Yau, S.-T. & Vekilov, P. G. (2000). Quasi-planar nucleus structure in apoferritin crystallisation. *Nature* **406**, 494-497.

Novel technique for determinations of protein nucleation rates

The techniques typically used for studies of nucleation of new phases in small molecule, polymer or colloid solutions are inapplicable, or would produce ambiguous results if applied to proteins. Hence, we developed a novel method with the following main features (22): (a) For experiment statistics of the intrinsically stochastic process, 400 trials were carried out simultaneously under identical conditions. (b) Nucleation was separated from the ensuing crystal growth by decreasing supersaturation after a preset time. (c) Heterogeneous nucleation was eliminated from the experiment statistics by monitoring the dependence of the number of nucleated crystals on the time allocated for nucleation. Detailed description of the experimental set up, schematically depicted in Fig. 1, and procedures is available in (22)

Publications:

Galkin, O., and P. G. Vekilov. 1999. Direct determination of the nucleation rate of protein crystals. *J. Phys. Chem.* 103:10965-10971.

Miniaturized technique for determinations of the phase boundary–the temperature dependence of solubility

We have developed a miniaturized (volume of crystallizing solution < 100 μl) technique for determinations of protein solubility as a function of temperature. After nucleation, crystals are detected by the light they scatter. Then the temperature at which a solution with the initial concentration is in equilibrium with the crystals is sought by stepwise, equilibrium dissolution of the crystals. The approach to solubility from the side of dissolution provides for higher accuracy of the determinations. The method was used to determine the temperature dependence of the solubility of human hemoglobin (Hb) C, for which high-resolution x-ray crystallography data are needed to understand the structural basis for the drastically different *in-vivo* aggregation /crystallization behavior of β6 Hb mutants. The temperature dependence of the solubility allowed

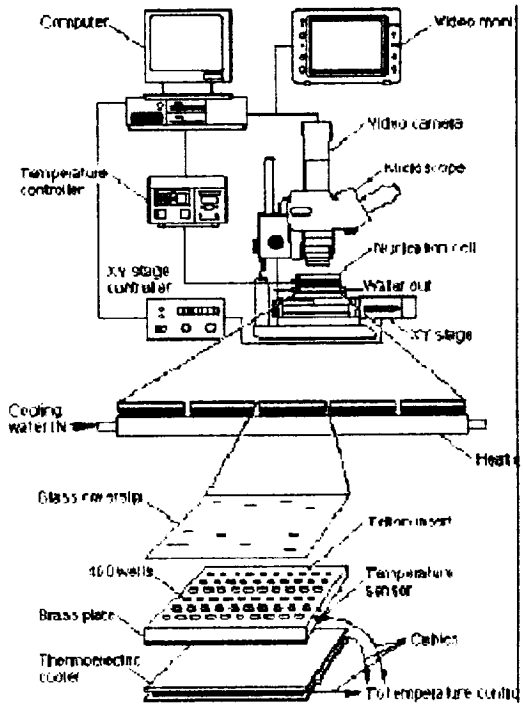

Fig. 1.

determination of the heat of crystallization using Van't Hoff's equation.

Publications:

Feeling-Taylor, A. R., R. M. Banish, R. E. Hirsch, and P. G. Vekilov. 1999. Miniaturized scintillation technique for protein solubility determinations. *Rev. Sci. Instr.* 70:2845-2849.

3. Proteins studied in PI's laboratory

Using the techniques discussed above, we have studied the following proteins:

- *Ferritin*, an iron-transport protein (23, 24). Crystallization conditions, leading to diffraction resolution of 1.8 Å have been developed in our laboratory (25). We used this protein for our investigation of the fundamental molecular-level mechanisms of growth and defect formation at the molecular level.
- *Apoferritin*, the hollow shell of ferritin. The crystallization mechanisms of this protein are very similar to those found for ferritin, however, the rates are faster by about a factor of five.
- *Thaumatin*, a sweet protein from the African shrub Thaumatococcus danielii easily crystallizes in the presence of tartarate (26). We used this protein after purification by ion exchange chromatography and found significant deviation of the thermodynamics and kinetics parameters from those reported before.
- *Hemoglobin C, human* [Hirsch, 1985 #211]. One of the β6 human hemoglobin mutants with distinct aggregation behavior *in-vivo*. The structural bases of the solution stability and aggregation of the Hb mutants cannot be discerned from the available molecular structures. We achieved improvement in the diffraction resolution of this protein by 0.3-0.4 Å by growing the crystals at carefully controlled and constant temperature Further AFM results suggest additional pathways of improvement of the crystallization condition, see Section A.12 below.
- *Hemoglobin S, human* (27). Another β6 mutant of human hemoglobin whose polymerization *in vivo* in deoxy state underlies the sickle cell anemia. We are currently collecting the first molecular resolution images of this process. Nucleation kinetics studies indicate that the process of nucleation of the primary fibers follows Poisonian statistics. Pathways for control of this process that may potentially have therapeutic consequences are currently investigated
- *Lumazine/riboflavin synthase*, from *Bacillus subtilis* (28, 29). These studies are in collaboration with colleagues form TU – Munich and aim to develop techniques to reproducibly attach enzymes to semiconductor substrates that would allow addressing of individual protein molecules for, e.g., data storage devices.
- *Lysozyme, from hen egg white.* This easily available and purifiable protein was used for the nucleation kinetics studies, which required large volumes of supersaturated protein solutions.

4. Nonlinear dynamics of growth steps in the mixed kinetics-bulk transport regime

Using atomic force microscopy and differential phase shifting interferometry techniques during crystallization of the proteins ferritin, apoferritin, lysozyme, thaumatin and hemoglobin C, we found that that the local growth rates and step velocities and densities are not steady but fluctuate by several times their average values, even under steady external conditions. The step density variations indicate that these fluctuations occur through the formation and decay of step bunches. Based on scaling arguments and numerical simulations, we argue that the fluctuations are the response of the coupled (bulk) transport and kinetics (of interacting steps on the interface) to finite amplitude perturbations. In search of means to reduce and eliminate his unsteady behavior that may be detrimental to the crystals' quality, we accelerated the bulk transport towards the interface by forced solution flow. We found that this results in *lower* fluctuation amplitudes. AFM results on step bunching for ferritin and apoferritin indicate that the response of these transport-controlled systems to faster or slower bulk transport is

opposite to that of lysozyme. We found that step bunching and kinetics fluctuations are suppressed if the relative weight of transport in the overall process control is *higher*. Our observations with all studied proteins indicate that the step bunching dynamics is controlled by the kinetic Peclet number, i.e., the relative weight of bulk transport and interface kinetics in the growth process. This number can be modified by either forced solution flow or suppression of buoyancy-driven convection, through growth under reduced gravity or in viscous media. Hence, our model provides a rationale for the choice of specific transport conditions to minimize unwanted instabilities (30).

5. Molecular mechanisms of crystallization

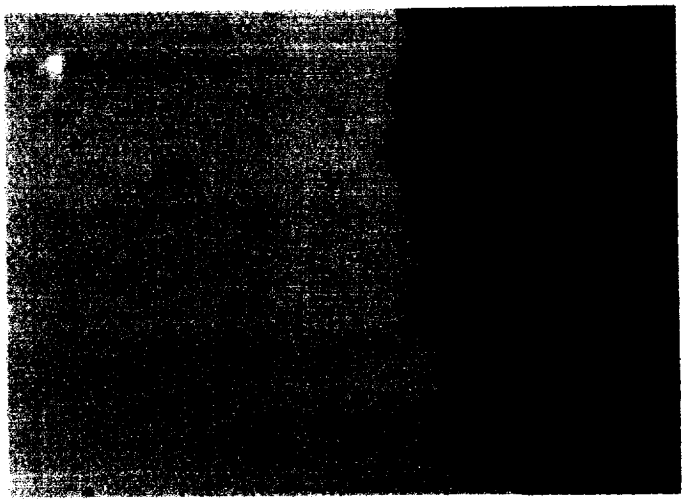

Fig. 2. Molecular structure of a growth step: apoferritin

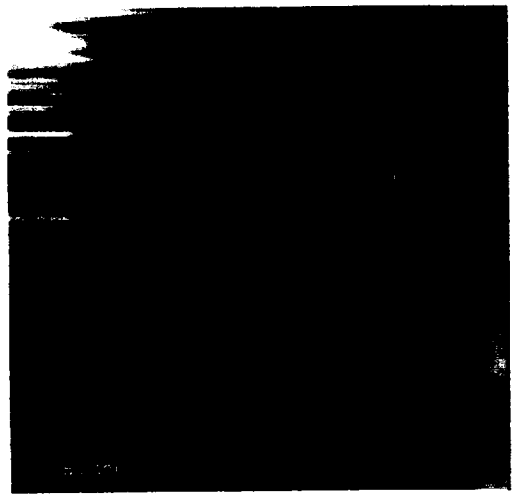

Fig. 3. Molecular structure of growth steps: hemoglobin C.

For studies of the molecular mechanisms of crystal growth from supersaturated environments, we chose crystallization of ferritin, apoferritin and hemoglobin C, Figs. 2 and 3. The AFM images revealed that for all three studied proteins, the periodicity within a molecular rows the layer thickness are in excellent agreement with the X-ray structure data (23, 24) for the respective proteins.

The kinks at a step are the only sites at which a solute molecule may be incorporated into the crystal (31). The kink density is a one of the ***fundamental properties*** of the crystal surface (32) and the value for apoferritin is 3.5. From the $\bar{n}_k$ we can evaluate ***the intermolecular bond energy,*** ϕ (32). We get $\phi = 3.2\ k_B T$ and found that accounting for second and third neighbor contributions, ϕ may be lowered by at most 10 % (33).

While the kink density is a thermodynamic growth variable that characterizes the affinity of the crystal to the solute molecules, the kinetics of incorporation are reflected by the flux of molecules into a growth site. To monitor these fast incorporation events, we disabled the slow scanning axis of the AFM and found that the net ***frequency of attachment of molecules to kinks*** is $f = 0.065\ s^{-1}$, or one molecule /15 s (21).

Incorporation of molecules into growth sites results in step propagation. At supersaturation of 1.1, the step velocity for apoferritin is 0.26 nm/s (21). The product $a(1/\bar{n}_k)f$ determined at the same conditions should equal this step velocity. Substituting, we get 0.24 nm/s. The closeness of the predicted and actual values indicates that kink density along the dense crystallographic directions and net frequency of attachment to a kink ***are the fundamental variables*** that ***fully determine*** the step propagation during crystal growth.

Publications:

Yau, S.-T., Thomas, B. R. & Vekilov, P. G. (2000). Molecular mechanisms of crystallization and defect formation. *Phys. Rev. Lett* **85**, 353-356.

Yau, S.-T., Petsev, D. N., Thomas, B. R. & Vekilov, P. G. (2000). Molecular-level thermodynamic and kinetic parameters for the self-assembly of apoferritin molecules into crystals. *J. Mol. Biol.* **303**, 667-678.

6. Imaging of adsorbed molecules clusters and aggregates and molecular mechanisms of defect formation

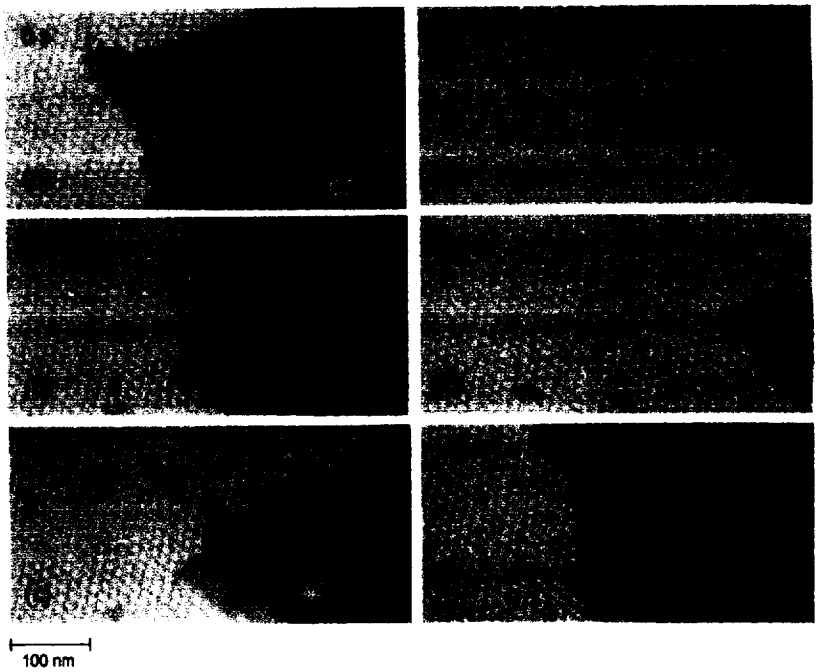

Fig. 4

We monitored the interactions between two advancing steps and the adsorbed impurity species. We identified the impurities as ***apoferritin dimers*** shaped as two bound monomer spheres, and found that the dimer surface concentration is 22 dimers/$\mu m^2 = 2.2 \times 10^8$ dimers/cm^2 [Yau, 2000 #565]. This is 100 – 1000-fold higher than typical dimer concentrations in the bulk solution (25). The dimers are strongly adsorbed on the surface and impede advancing growth steps (34). Fig. 4 shows that after the ***dimer*** C1 in Fig. 4a is buried into the lattice by a new growing layer, no monomer molecules are deposited directly above it. We attribute this to the lattice ***strain*** that the dimer introduces. Furthermore, no molecules are deposited above the vacancies, compare Figs. 4a and c, and ***stacks of vacancies*** up to 10 layers high form (21). An AFM movie, showing the reversible and of single molecules, the dynamic equilibrium that ensues when a step reaches two nearby defects, and the replication and evolution of defects is available as an animated GIF file at **http://www.cmmr.uah.edu/protein/movies.html**

Publications:

Yau, S.-T., Thomas, B. R. & Vekilov, P. G. (2001). Molecular mechanisms of microheterogeneity-induced defect formation in ferritin crystallization. *Proteins: Structure, Function, Genetics* **43**, 343-352.

Petsev, D. N., Thomas, B. R., Yau, S.-T. & Vekilov, P. G. (2000). Interactions and Aggregation of Apoferritin Molecules in Solution: Effects of Added Electrolytes. *Biophysical J.* **78**, 2060-2069.

7. Defects, strain and mosaicity

The ***strain*** caused by the various ***defects*** in a stack is evidenced in Fig. 5 showing ~ 1-2 nm shifts of the molecules around the defects from their crystallographic positions (intermolecular distance is ~ 13 nm). The balance between this elastic strain and the surface energy between potential mosaic blocks determines the existence of a critical size for the onset of ***mosaicity*** (35, 36). Indeed, mosaic blocks ~ 10-20 μm wide were observed for ferritin crystals larger than ~ 200 μm growing from solutions 2-3 months old in which the concentration of the dimers is higher (25). Growth steps were confined within the individual blocks and the growth of each block was independent of the others.

For further evidence for impurity induced mosaicity, we monitored the growth and dissolution of lysozyme crystals. As with ferritin, typical impurities for this protein are covalently bound dimers at ~ 1 % of the dry protein mass. They cannot be fully removed, recur after purification and readily incorporate into crystals. The sequence in Fig. 6 shows subsequent stages of dissolution of a crystal grown at a high supersaturation of $\Delta\mu/k_BT$ = 3.65 from a solution containing 1.5 % (w/w dry protein mass) of the lysozyme dimer. Dissolution of the heavily mosaic crystal, Fig. 5a, reveals that below ~ 170 μm, Fig. 5c, the crystal consists of a single block. This is the ***critical size*** for the onset of mosaicity, close to earlier estimates (36). Crystal grown from solutions containing lower impurity amounts did not reveal such mosaic structure. This allows us to correlate the mosaicity to the lattice strain introduced by the impurity incorporation. As discussed in Section B.3. above, higher ***mosaicity*** may be associated with poorer diffraction resolution.

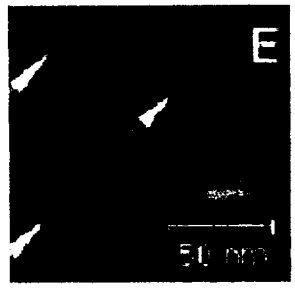

Fig. 5

Fig. 6

Publications:

Yau, S.-T., Thomas, B. R. & Vekilov, P. G. (2000). Molecular mechanisms of microheterogeneity-induced defect formation in ferritin crystallization. *Proteins: Structure, Function, Genetics* **43**, 343-352.

8. Lower Incorporation of Impurities in Ferritin Crystals by Suppression of Convection: Modeling Results

We have developed an axi-symmetric time-dependent numerical model of the diffusive-convective transport of a crystallizing protein and an impurity, in an isothermal crystal growth system *at standard and zero gravity*. We model crystallization of ferritin, a protein with M_w=440,000, and its most abundant impurity, the protein's native dimer. The diffusivities of the protein and the dimer and the kinetic coefficients for crystallization and impurity incorporation are available. The model assumes the geometry of a cylindrical vessel used in protein crystallization trials on earth and in space, the DCAM. At terrestrial gravity, buoyancy-driven convection with a maximum velocity of 12 μm/s enhances the supply of both protein and impurity, Fig. 7a. In the absence of convection, e.g., at 0g, the diffusion depletion zone is wider and the interfacial concentrations drop significantly, see Fig. 7b. The lower diffusivity of the larger dimer results in its incorporation at 0g lower by factors of 2 – 3 than on earth. The three-dimensional computational scheme used here allows direct comparisons of these results with space and laboratory experimental data. The two data sets agree quantitatively, suggesting that in some cases, the improved quality of space grown crystals as compared to the earth grown controls may be due to the suppressed supply of larger impurities.

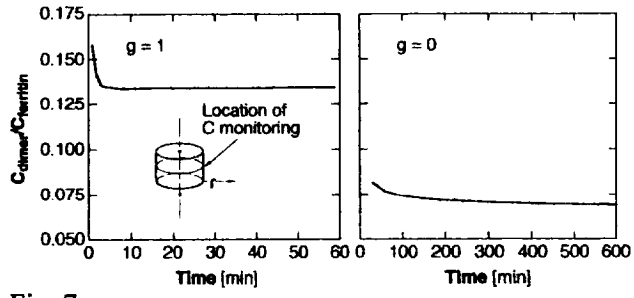

Fig. 7

Publications:

Lin, H., Petsev, D. N., Yau, S.-T., Thomas, B. R. & Vekilov, P. G. (2001) Lower Incorporation of Impurities in Ferritin Crystals by Suppression of Convection: Modeling Results. *Crystal Growth and Design* **1**, 73-79

9. Heterogeneity characterization and purification

Sections A.6and 7 above the mechanism by which *impurities* may cause defects and severely *deteriorate* the perfection of the growing crystals. We investigated in detail the ***incorporation of impurities and their effects on the crystal growth*** and perfection using apoferritin. By intentionally adding a number of proteins to previously purified solutions of apoferritin, we found that the ***naturally occurring oligomers*** of the protein are most extensively incorporated into the crystals (37). The effect of naturally occurring oligomers on the crystallization of isolated, microhomogeneous apoferritin monomers (24 subunits, Mr = 440,000) was investigated in detail (25). SDS PAGE analysis and immunoblotting showed that commercial apoferritin was free of foreign proteins (>99.9% w/w). The quaternary structure of apoferritin oligomers that form prior to the addition of precipitant was analyzed in native 4-15% T (1-2% C) gradient PAGE. Optical densitometry of these gels showed that oligomers (> 24 subunit monomer) constituted approximately 45% w/w of the total apoferritin. The primary oligomeric contaminants were dimers (48 subunits) with 35% w/w, and several bands constituting trimers (~72 subunits) with 10% w/w. Directly determined physical molecular weights (Mw) and conformational data for oligomers obtained by analytical gel filtration Fast Protein Liquid Chromatography separations utilizing UV and multi-angle laser light scattering detectors (GF-FPLC-MALLS) confirmed and expanded the native PAGE results. This technique allowed the discovery of large oligomers (Mw = 5,000,000 and 80,000,000) present in concentrations < 1% w/w. Semi-preparative GF-FPLC was used to quantitatively reduce oligomer contamination to 5% w/w, and to produce 0.25 g of microhomogeneous monomers from 0.5 g APO. Crystallization from microhomogeneous monomer solutions yielded large crystals 0.5-1.0 mm in size. These crystals yielded X-ray diffraction resolution of 1.8 Å, better than the best published value of 1.95 Å (24). Reconstitutive experiments in which isolated oligomers were added to monomer preparations showed that dimers perturb the growth habit and reduce the crystal growth, without significantly affecting the nucleation . On trimer addition, the nucleation was increased and the crystal growth slowed. Addition of cadmium sulfate(see below) to unpurified apoferritin did not affect the nature or quantity of the oligomers. These effects of oligomers on crystallization underline ***microheterogeneity as a critical factor in crystallization*** of this, and perhaps other, protein systems (37-39).

Publications:

Thomas, B. R., Chernov, A. A., Vekilov, P. G. & Carter, D. C. (2000). Distribution coefficients on protein impurities in ferritin and lysozyme crystals. Self-purification in microgravity. *J. Crystal Growth* **211**, 149-156.

10. Interactions and aggregation of protein molecules in solution

We have studied the ***structure of the protein species*** and the protein-protein interactions in solutions containing two apoferritin molecular forms, monomers and dimers, in the presence of Na^+ and Cd^{2+} ions (40), *attached to proposal*. We combined ***static and dynamic light scattering*** techniques with protein liquid chromatography and atomic force microscopy (AFM). Size-exclusion chromatography was used to isolate these two protein fractions. The sizes and shapes of the monomers and dimers were determined by dynamic light scattering and AFM. While the monomer is an apparent sphere with a diameter corresponding to previous x-ray crystallography determinations, the ***dimer shape*** corresponds to two, bound monomer spheres. Static light scattering was applied to characterize the interactions between solute molecules of monomers and dimers in terms of the second osmotic virial coefficients. The results for the monomers indicate that Na^+ ions cause strong intermolecular repulsion even at concentrations higher than 0.15 M, ***contrary to the predictions*** of the commonly applied Derjaguin-Landau-Verwey-Overbeek theory (41). We argue that the reason for such behavior

is ***hydration force*** due to the formation of a water shell around the protein molecules with the help of the sodium ions. The addition of even small amounts of Cd^{2+} changes the repulsive interactions to attractive but does not lead to oligomer formation, at least at the protein concentrations used. Thus, the two ions provide examples of strong specificity of their interactions with the protein molecules. In solutions of the apoferritin dimer, the molecules attract even in the presence of Na^{+} only, indicating a change in the surface of the apoferritin molecule. In view of the strong repulsion between the monomers, this indicates that the dimers and higher oligomers form only after partial denaturation of some of the apoferritin monomers. These observations suggest that ***aggregation and self-assembly of protein molecules*** or molecular subunits may be driven by forces other than those responsible for crystallization and other phase transitions in the protein solution.

Publications:

Petsev, D. N., Thomas, B. R., Yau, S.-T., Tsekova, D., Nanev, C., Wilson, W. W. & Vekilov, P. G. (2000). Temperature-independent Solubility and Interactions between Apoferritin Monomers and Dimers in Solution. *J. Crystal Growth* **232**, 21-29 (2001).

Petsev, D. N., Thomas, B. R., Yau, S.-T. & Vekilov, P. G. (2000). Interactions and Aggregation of Apoferritin Molecules in Solution: Effects of Added Electrolytes. *Biophysical J.* **78**, 2060-2069.

Petsev, D. N. & Vekilov, P. G. (2000). Evidence for Non-DLVO Hydration Interactions in Solutions of the Protein Apoferritin. *Phys. Rev. Lett.* **84**, 1339-1342.

11. Control of protein crystal nucleation

We carried out two types of determination of the homogeneous nucleation rates J of lysozyme crystals: (i) at constant temperature $T = 12.6$ °C and (ii) at constant protein concentration C. We found that for the chosen model protein system, crystal nucleation is an intrinsically stochastic process. In this respect, protein nucleation is similar to nucleation of simple liquids or water-soluble inorganic materials. Multiple repetitions of a nucleation experiment under identical conditions allow reproducible determinations of its characteristic rates. Although the dependencies of the homogeneous nucleation rate on protein and precipitant concentration are similar to those found in small-molecule systems, the nuclei consist of only a few molecules. Strictly speaking, this ***precludes*** direct applications of ***classical nucleation theory*** to the studied system. With increasing supersaturation, imposed by increasing protein or precipitant concentrations, the nucleus size takes discrete values of ***10 or 11, then 4 or 5, then 1 or 2 molecules*** (42). This leads to a broken dependence of the nucleation rate on supersaturation that is beyond the predicting capabilities of classical nucleation theories. For further details and implications of these results, see (42).

The presence of a liquid-liquid (L-L) phase boundary hidden below the liquidus (solubility) line in the phase diagram of the protein solution has a profound effect on J. We show that in the vicinity of the L-L boundary J is enhanced by factors of 6 to 20. In the region of liquid-liquid demixing below the L-L boundary, the nucleation rate is lower than at the maximum (43), *attached to proposal*. The found correlation allows

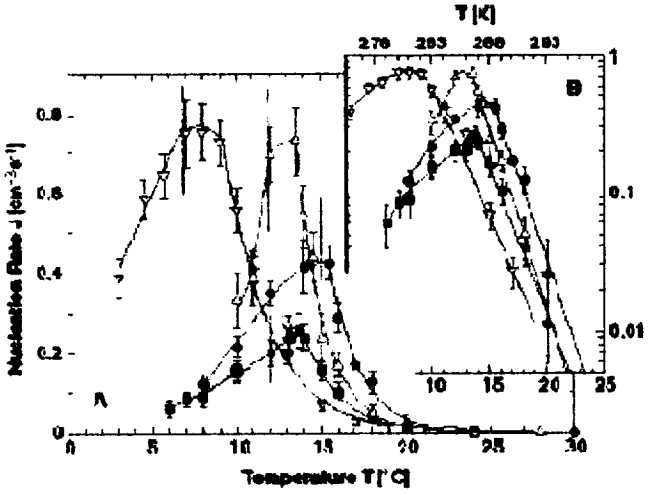

Fig. 8. Closed symbols: no additives, lysozyme concentration C_{lys} ¦ - 50 mg/mL, and ? - 80 mg/mL; open symbols C_{lys} = 50 mg/ml, ∇ - 5 % (vol.) glycerol, ? - 0.2 % (w/v) polyethylene glycol 5 000; vertical dotted lines denotes temperatures of liquid-liquid demixing.

control of the nucleation rate of protein crystals by using additives that shift the L-L boundary. Fig. 8 shows that glycerol (open triangles) and polyethylene glycol (PEG) (open inverted triangles), both of them do not specifically bind to proteins (44-46), shift this phase boundary and significantly suppress or enhance the crystal nucleation rates. No simple correlation exists between the action of PEG on the phase diagram and the nucleation kinetics. The control mechanism does not require changes in the protein concentration, the acidity and ionicity of the solution. The effects of the two additives on the phase diagram depend on their concentration and this provides for further tuning of nucleation rates (43).

The mechanism of nucleation control illustrated above is not confined to the two studied additives. More importantly, this control mechanism does not require variations of the solution ionicity, acidity, temperature or protein concentration.

Publications:

Galkin, O., and P. G. Vekilov. 1999. Direct determination of the nucleation rate of protein crystals. *J. Phys. Chem.* 103:10965-10971.

Galkin, O., and P. G. Vekilov. 2000. Are nucleation kinetics of protein crystals similar to those of liquid droplets? *J. Amer. Chem. Soc.* 122:156-163.

Galkin, O. & Vekilov, P. G. (2000). Control of protein crystal nucleation around the metastable liquid-liquid phase boundary. *Proc. Natl. Acad. Sci. USA* 97(12), 6277-6281.

O. Galkin and P.G. Vekilov, 2001 "Nucleation of protein crystals: critical nuclei, phase behavior, and control pathways," J. Crystal Growth **232**, 63-76.

12. Rational approach to optimization of crystallization conditions: Hb C solubility; AFM visualization of aggregates

High-resolution x-ray crystallography data for the numerous hemoglobin mutants are needed to understand the structural basis for their drastically different *in-vivo* aggregation /crystallization behavior. In search for better crystallization conditions for one of the β6 mutants, that are related to some severe pathological conditions, we worked with Hemoglobin C, in which glutamic acid in the β6 position is replaced by a lysine.

To determine the protein solubility, we used the miniaturized device discussed above. The solubility data were used to design a novel strategy for growing hemoglobin C crystals for x-ray structure studies by the temperature gradient technique (47). In this method, a linear temperature gradient is set across a X-ray capillary. The high temperature setting is chosen such that it provides for supersaturation at which crystal nucleation occurs, on the average, over 2-4 days. The low temperature value is selected to be 12 °C so that the solution is slightly undersaturated. This temperature gradient typically results in 1 or 2 crystals in the high temperature zone The crystals grown by this method *diffracted to 1.8 Å resolution.* This is an improvement over previous studies, in which batch-grown Hb C crystals diffracted to 2.1 Å.

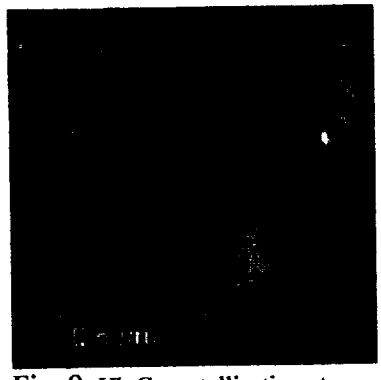

Fig. 9. Hb C crystallization at high protein concentration

In search of pathways leading to further improvement the diffraction resolution, we studied the molecular level growth processes using the atomic force microscope as discussed above. Fig. 9 and many other similar images showed that the roughness of the growth steps propagating on the face of the growing crystal is of the scale of 1 molecule, i.e., growth proceeds by the incorporation of *single hemoglobin C molecules*. This indicates the need for pre-formed aggregates in the nutrient medium *is not* the factor limiting the resolution. If the concentration of Hb C is increased, the AFM

images, Fig. 8, reveal the formation *of amorphous aggregates* of the protein that adsorb on the surface and cause vacancies and strain, similar to behavior of ferritin clusters discussed above. We attribute the relatively poor diffraction resolution to the incorporation of these aggregates. Hence, our efforts to improve the crystallization conditions have centered on finding solution compositions that prevent aggregate formation.

13. References

1. Binnig, G., Gerber, C., Stoll, E., Albrecht, R. T. & Quate, C. F. (1987) *Europhys. Lett* **3,** 1281-1286.
2. Yip, C. M. & Ward, M. D. (1996) *Biophysical J.* **71,** 1071-1078.
3. Kuznetsov, Y. G., A.J.Malkin, Land, T. A., DeYoreo, J. J., Barba, A. P., Konnert, J. & McPherson, A. (1997) *Biophys. J.* **72,** 2357-2364.
4. Yip, C. M., DePhelippis, M. R., Frank, B. H., Brader, M. L. & Ward, M. D. (1998) *Biophysical J.* **75,** 1172-1179.
5. Li, M., Nadarajah, A. & Pusey, M. L. (1999) *Acta Cryst. Section D* **55,** 1036.
6. Li, H., Perozzo, M. A., Konnert, J. H., Nadarajah, A. & Pusey, M. L. (1999) *Acta. Crystallogr. Section D* **55,** 1023-1035.
7. Hansma, H. G. & Hoh, J. H. (1994) *Annu. Rev. Biophys. Biomol. Struct.* **23,** 115-139.
8. Engel, A., Gaub, H. E. & Müller, D. J. (1999) *Curr. Biol* **9,** R133-R136.
9. Kuipers, L., Hoogeman, M. & Frenken, J. (1993) *Phys. Rev. Letters* **71,** 3517-3520.
10. Kuipers, L., Hoogeman, M. S. & Frenken, J. W. M. (1995) *Phys. Rev. B* **52,** 11387-11397.
11. Giesen-Seibert, M., Schmitz, F., Jentjens, R. & Ibach, H. (1995) *Surf. Sci.* **329,** 47-60.
12. Giesen, M., Schulze Icking-Konert, G., Stapel, D. & Ibach, H. (1996) *Surface Science* **366,** 229-238.
13. Hansma, P. K., Cleveland, J. P., Radmacher, M., Walters, D. A., Hillner, P., Bezanilla, M., Fritz, M., Vie, D., Hansma, H. G., Prater, C. B., Massie, J., Fukunaga, L., Gurley, J. & Elings, V. (1994) *Appl. Phys. Lett.* **64,** 1738-1740.
14. Noy, A., Sanders, C. H., Vezenov, D. V., Wong, S. S. & Lieber, C. M. (1998) *Langmuir* **14,** 1508-1511.
15. Möller, C., Allen, M., Elings, V., Engel, A. & Müller, D. J. (1999) *Biophys. J.* **77,** 1150-1158.
16. Yau, S.-T. & Vekilov, P. G. (2000) *Nature* **406,** 494-497.
17. Giesen-Seibert, M., Jentjens, R., Poensgen, M. & Ibach, H. (1993) *Phys. Rev. Letters* **71,** 3521-3524.
18. Poensgen, M., Wolf, J., Frohn, J., Giesen, M. & Ibach, H. (1992) *Surface Science* **274,** 430-440.
19. Kitamura, N., Lagally, M. G. & Webb, M. B. (1993) *Phys. Rev. Lett* **71,** 2081-2085.
20. Swartzentruber, B. S., Mo, Y.-W., Kariotis, R., Lagally, M. G. & Webb, M. B. (1990) *Phys. Rev. Lett.* **65,** 1913-1916.
21. Yau, S.-T., Thomas, B. R. & Vekilov, P. G. (2000) *Phys. Rev. Lett* **85,** 353-356.
22. Galkin, O. & Vekilov, P. G. (1999) *J. Phys. Chem.* **103,** 10965-10971.
23. Lawson, D. M., Artymiuk, P. J., Yewdall, S. J., Smith, J. M. A., Livingstone, J. C., Trefry, A., Luzzago, A., Levi, S., Arosio, P., Cesareni, G., Thomas, C. D., Shaw, W. V. & Harrison, P. M. (1991) *Nature* **349,** 541-544.

24. Hempstead, P. D., Yewdall, S. J., Fernie, A. R., Lawson, D. M., Artymiuk, P. J., Rice, D. W., Ford, G. C. & Harrison, P. M. (1997) *J. Mol. Biol* **268,** 424-448.
25. Thomas, B. R., Carter, D. & Rosenberger, F. (1997) *J. Crystal Growth* **187,** 499- 510.
26. Kuznetov, Y. G., Malkin, A. J., Geenwood, A. & McPherson, A. (1995) *J. Struct. Biol.* **114,** 184-196.
27. Eaton, W. A. & Hofrichter, J. (1990) in *Advances in protein chemistry*, eds. Anfinsen, C. B., Edsal, J. T., Richards, F. M. & Eisenberg, D. S. (Academic Press, San Diego), Vol. 40, pp. 63-279.
28. Bacher, A., Baur, R., Eggers, U., Harders, H., Otto, M. K. & Schnepple, H. (1980) *J. Biol. Chem.* **255,** 632-637.
29. Bacher, A., Weinkauf, S., Bachmann, L., Ritsert, K., Baumeister, W., Huber, R. & Ladenstein, R. (1992) *J. Mol. Biol.* **225,** 1065-1073.
30. Vekilov, P. G. & Alexander, J. I. D. (2000) *Chem. Rev.* **100,** 2061-2089.
31. Kaischew, R. (1936) *Z. Phys.* **102,** 684-690.
32. Burton, W. K., Cabrera, N. &. Frank, F.C. (1951) *Phil. Trans. Roy. Soc. London Ser. A* **243,** 299- 360.
33. Yau, S.-T., Petsev, D. N., Thomas, B. R. & Vekilov, P. G. (2000) *J. Mol. Biol.* **303,** 667-678.
34. Cabrera, N. & Vermileya, D. A. (1958) in *Growth and Perfection of Crystals*, eds. Doremus, R. H., Roberts, B. W. & Turnbul, D. (Wiley, New York).
35. Chernov, A. A. (1998) *Acta Crystallographica Section A* **54,** 859-872.
36. Chernov, A. A. (1999) *J. Crystal Growth* **196,** 524-534.
37. Thomas, B. R., Chernov, A. A., Vekilov, P. G. & Carter, D. C. (2000) *J. Crystal Growth* **211,** 149-156.
38. Thomas, B. R., Vekilov, P. G. & Rosenberger, F. (1996) *Acta Crystallogr. Section D* **52,** 776-784.
39. Thomas, B. R., Vekilov, P. G. & F. Rosenberger (1998) *Acta Crystallogr. Section D* **54,** 226-236.
40. Petsev, D. N., Thomas, B. R., Yau, S.-T. & Vekilov, P. G. (2000) *Biophysical J.* **78,** 2060-2069.
41. Petsev, D. N. & Vekilov, P. G. (2000) *Phys. Rev. Lett.* **84,** 1339-1342.
42. Galkin, O. & Vekilov, P. G. (2000) *J. Amer. Chem. Soc.* **122,** 156-163.
43. Galkin, O. & Vekilov, P. G. (2000) *Proc. Natl. Acad. Sci. USA* **97,** 6277-6281.
44. Lee, J. C. & Lee, L. L. Y. (1981) *J. Biol. Chem.* **256,** 625-631.
45. Rariy, R. V. & Klibanov, A. M. (1997) *Proc. Natl. Acad. Sci. USA* **94,** 13520-13523.
46. Farnum, M. & Zukoski, C. (1999) *Biophys J* **76,** 2716-26.
47. Rosenberger, F., Howard, S. B., Sowers, J. W. & Nyce, T. A. (1993) *J. Crystal Growth* **129,** 1-12.